CrossMark

ORIGINAL PAPER

# Study of the Irreversibility Line of GdBa$_2$Cu$_3$O$_{7-\delta}$ Added with Nanosized Ferrite CoFe$_2$O$_4$

H. Basma[1] · R. Awad[1,2] · M. Roumié[3] · S. Isber[4] · S. Marhaba[1] · A. I. AbouAly[2]

**Abstract** (CoFe$_2$O$_4$)$_x$ GdBa$_2$Cu$_3$O$_{7-\delta}$ superconducting samples were synthesized using a conventional solid-state reaction technique with $0 \leq x \leq 0.1$ wt%. Characterization of the prepared samples was carried out using X-ray powder diffraction (XRD) and scanning electron microscopy (SEM). The effect of adding CoFe$_2$O$_4$ to the Gd-123 phase, which acts as a flux pinning center, was investigated by measuring the ac magnetic susceptibility at different applied dc magnetic fields. Both the superconducting transition temperature $T_c$ and the critical current density $J_c$ increased up to $x = 0.01$ wt%, and then, they decreased with further increase in $x$. The temperature dependence of the irreversibility line was investigated by the logarithmic plot of the irreversibility field $H_{irr}$ versus $(1 - T_{irr}/T_c(0))$. This plot shows a crossover at a field of 1000 Oe, indicating 3D to 2D flux creep fluctuations. Furthermore, the $H_{irr}-T$ curves are well fitted according to a theoretical model pro-

✉ H. Basma
  hadibassma@gmail.com

1 Physics Department, Faculty of Science, Beirut Arab University (BAU), Beirut, Lebanon

2 Physics Department, Faculty of Science, Alexandria University, Alexandria, Egypt

3 Accelerator Laboratory, Lebanese Atomic Energy Commission, CNRS, Beirut, Lebanon

4 Department of Physics, American University of Beirut, PO Box 11-0236, Beirut, Lebanon

posed by Matsushita, based on the depinning mechanism caused by thermally activated flux creep.

## 1 Introduction

Gd-123 is considered as one of the most promising materials among the currently known high-temperature superconductors (HTSCs). It possess high superconducting transition temperature (around 90 K) [1], high critical current density $J_c$ values at high magnetic fields [2, 3], high ability to trap the magnetic field up to 2.0 T at 77 K [4], relative low crystalline anisotropy, and well-developed pinning properties in the magnetic field [5]. However, Gd-123 showed a rapid decrease in its critical current density as both the temperature and the magnetic field increase. An effective way to overcome this problem is the enhancing of its flux pinning capabilities by irradiation [6–10], chemical substitution [11, 12], and nanoparticle addition [13–15].

In the mixed state, magnetic field penetrates into the superconductor matrix in the form of magnetic flux vortices. The core of vortices is in a non-superconducting state. All vortices in superconductors are subjected to Lorentz force because they carry a magnetic moment and therefore move through the crystal. These vortices interact with supercurrent, causing an interaction with the crystal lattice. This leads to dissipation of their energy and electric resistance appears [6]. One of the most effective ways to increase the flux pinning is the nanosized particle addition. A wide variety of HTSCs were pinned [16–24], and most of the results

showed that the superconducting parameters were improved at low amounts of nanosized particle additions. On the other hand, high amounts reduced the formation of a superconducting phase. It was shown, from previous studies, that the addition of nanosized $ZrO_2$, $SnO_2$, and $(ZrO_2 + CoO)$ into the bulk superconductor $GdBa_2Cu_3O_{7-\delta}$ enhanced the flux pinning and consequently improved critical current density [25–27]. The effect of addition of $CoFe_2O_4$ on $GdBa_2Cu_3O_{7-\delta}$ was previously investigated by Awad et al. [28], and they found that the addition of $CoFe_2O_4$ up to 0.01 wt% enhanced the superconducting parameters.

The unusual behavior of HTSCs in a mixed state has attracted considerable attention. One of the attractive subjects in the last few years is the $H$–$T$ diagram of HTSCs. The boundary of the $H$–$T$ plane is called the irreversibility line, separating a magnetically irreversible, zero-resistance state ($J_c \neq 0$) from a reversible region with dissipative properties ($J_c = 0$). In the area below the irreversibility line, a high-temperature superconductor is characterized by a strong irreversible magnetic phenomenon which is similar to a conventional type II superconductor in the presence of pinning. However, the magnetic irreversibility disappears above this line and the high-temperature superconductor therefore can carry no supercurrent in this case. Many experimental techniques such as ac susceptibility, dc magnetization, and magnetomechanical effect are used to probe the irreversibility line. Apparently, the results from each method are slightly different from the others. They also depend on the sample size and other experimental parameters, such as the frequency and the value of dc fields in ac susceptibility measurement. The irreversibility line has been interpreted by many authors as the quasi-de Almeida–Thouless line, the depinning line, the vortex lattice melting line, and the vortex glass transition line. The magnetic irreversibility persists up to a well-defined temperature limit that depends on the applied field as well as on certain thermodynamic properties of the superconductors [29]. The magnetic irreversibility in type II superconductors originates from the movement of vortices which consequently overcome the imprisonment forces. In the region magnetically reversible, the vortices have enough energy and they can move freely, while in temperatures under $T_{irr}$, the mobility is restricted and the vortices remain trapped in the pinning center. Most of the studies interpreted the irreversibility line as a crossover in the dimensionality of the vortex ensemble. At low fields, the vortex lines maintain a 3D character whereas at high fields, there is a quasi-2D vortex fluctuation. A previous study conducted by Awad et al. [30] for $(ZnFe_2O_4)_xGdBa_2Cu_3O_{7-\delta}$ showed a crossover at $H = 500$ Oe from 3D to 2D vortex fluctuations.

In this work, the effect of $CoFe_2O_4$ addition on the Gd-123 superconductor using ac susceptibility measurements as a function of temperature of $(CoFe_2O_4)_xGdBa_2Cu_3O_{7-\delta}$,

$0 \leq x \leq 0.1$ wt%, at a frequency of 1 KHz in varying dc fields was studied.

## 2 Experimental Techniques

Nanosized $CoFe_2O_4$ powder was prepared by a chemical co-precipitation method as discussed in a previous work [28].

Superconducting samples of type $(CoFe_2O_4)_xGdBa_2Cu_3$ $O_{7-\delta}$, $0.0 \leq x \leq 0.1$ wt%, were prepared by the conventional solid-state reaction technique. First, the starting materials $Gd_2O_3$, $BaCO_3$, and $CuO$ (purity $\geq 99.9$) were crushed in an agate mortar and were sifted using a 125-$\mu$m sieve to get a homogeneous mixture. Then, the powder was subjected to a calcination process in air at 840 and 880 °C for 24 h each. The resultant powder was ground and sifted, and $x$ wt% of nanosized $CoFe_2O_4$ was added to the resulting powder. The powder was mixed for 1 h to ensure the homogeneous distribution of nanosized $CoFe_2O_4$ inside the sample. Subsequently, the mixed powder was pressed in a disc form (1.5 cm in diameter and about 0.3 cm in thickness). Afterwards, discs were sintered in air at 930 °C with a heating rate of 4 °C/min, and held at this temperature for 24 h. Then, the samples were cooled by a rate of 1 °C/min down to 450 °C and kept at this temperature for 10 h under oxygen flow to control the oxygen content of the final compounds. Finally, they were slowly cooled by a rate of 1 °C/min to room temperature. The characterization and superconductivity investigation of these samples were carried out using X-ray powder diffraction (XRD), scanning electron microscopy (SEM), electrical resistivity, and $I$–$V$ characteristics [31].

The ac magnetic susceptibility at different applied dc fields was measured using a Quantum Design Physical Properties Measurements System (PPMS) equipped with a
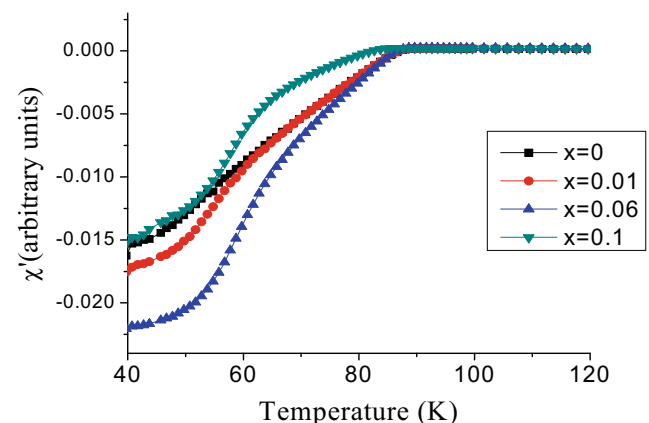


**Fig. 1** The real part of the magnetic susceptibility versus temperature at a field of 9 Oe for samples with $x = 0, 0.01, 0.06$, and 0.1 wt%

**Table 1** The values of $T_c$ and $n_1$ of the power relation obtained from (1) at low field ($H < 1000$ Oe), $n_2$ of the power relation obtained from (1) at high field ($H > 1000$ Oe), and the fitting parameters ($K$, $m$, and $\gamma$) according to (2) for $(CoFe_2O_4)_x GdBa_2Cu_3O_{7-\delta}$, $x = 0.00$, 0.001, 0.04, 0.06, 0.08, and 0.1 wt%

| Sample | $T_c$ | $n_1$ | $n_2$ | $K$ | $m$ | $\gamma$ |
|---|---|---|---|---|---|---|
| Co-0.00 | 89.59 | 1.43 | 4.92 | 89.59 | 0.0145 | 1.455 |
| Co-0.01 | 87.65 | 2.41 | 4.14 | 86.00 | 0.0145 | 1.455 |
| Co-0.04 | 82.14 | 2.50 | 6.15 | 88.00 | 0.0150 | 1.450 |
| Co-0.06 | 80.16 | 2.48 | 4.16 | 86.50 | 0.0145 | 1.475 |
| Co-0.08 | 79.13 | 2.78 | 4.80 | 86.00 | 0.0150 | 1.465 |
| Co-0.10 | 78.57 | 2.58 | 3.30 | 88.60 | 0.0150 | 1.475 |

9-T superconducting magnet. The system has a sensitivity of $1 \times 10^{-8}$ emu, an amplitude range of 0.005–15 Oe (peak), and a frequency range of 10 Hz–10 KHz, with a direct phase-nulling technique that measures and cancels background ac phase shifts at every measurement. The ac magnetic susceptibilities were measured on powder samples of typical masses of 200–300 mg placed in a 0.5 mm $\times$ 1.5 mm gelatin capsule which is tightly held at the bottom of the sample holder. These samples were subjected to seven different values of the external magnetic fields between 0 and 3000 Oe and temperature range of 40–120 K. The amplitude of the excitation magnetic field was set to 9 Oe in all runs at a fixed frequency of 1 KHz.

## 3 Results and Discussions

The analysis of nanosized $CoFe_2O_4$ powder by XRD showed that all the diffraction peaks can be indexed by the face center cubic structure of cobalt ferrite with space group Fd3m. The crystalline size, determined from XRD and TEM, was 8 nm [28]. The superconductivity investigation of the Gd-123 samples showed that the volume fraction, superconducting transition temperature, and critical current density were increased from 0 to 0.01 wt%, and then, they decreased with further increases in $x$ [28].
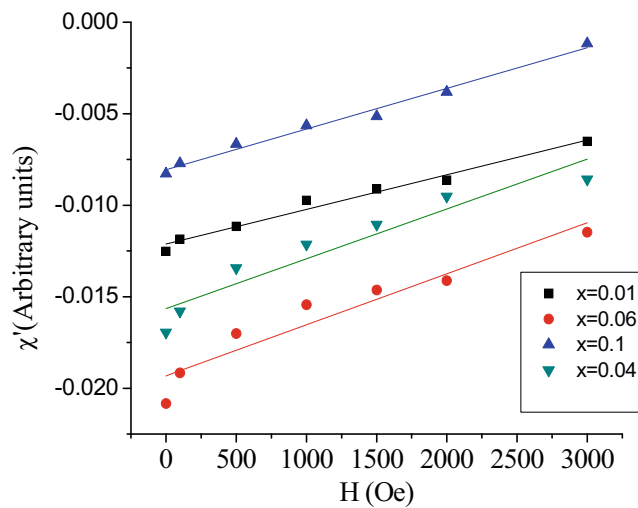
The real part of the ac magnetic susceptibility versus temperature at a field of 9 Oe for $(CoFe_2O_4)_x GdBa_2Cu_3O_{7-\delta}$, with $x = 0$, 0.01, 0.06, and 0.1 wt%, is shown in Fig. 1. Usually, the real part of ac magnetic susceptibility $\chi'$ of type II superconductors has two contributions. The first one is the sharp drop which is attributed to the transition within grains (intra) while the second is the gradual change, corresponding to the occurrence of the superconducting coupling between grains or matrix (inter). On the other hand, the Gd-123 samples show a different behavior where the intrinsic component of $\chi''$ shows a much stronger effect on the applied field [32]. This behavior is obtained as due to the response of $\chi''$ to the applied field just below the transition temperature $T_c$, where the intrinsic (grain) component arises. Namuco et al. [33] compared between the ac magnetic susceptibility of Y-123 and Gd-123, and the results showed that the Gd-123 showed a more sensitive ac magnetic susceptibility response. The magnetic and
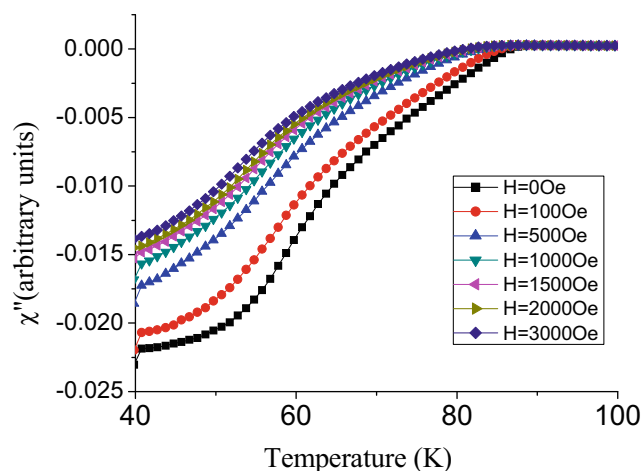


**Fig. 2** The real part of the magnetic susceptibility of samples with $x = 0.06$ wt% for applied dc field values 0 Oe $\leq H_{dc} \leq$ 3000 Oe
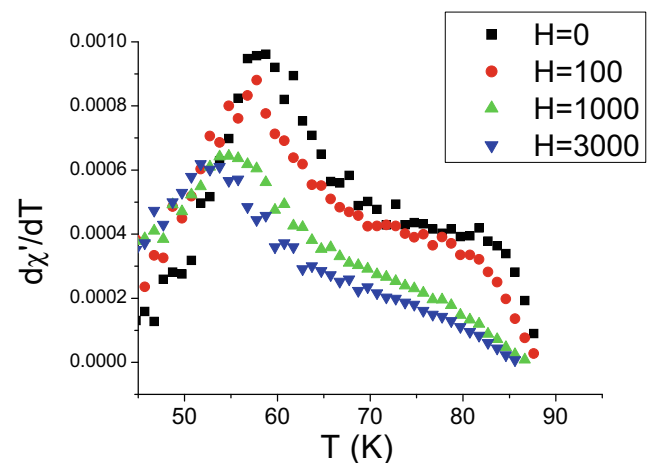


**Fig. 3** $d\chi'/dT$ versus temperature at $H = 0$, 100, 1000, and 3000 Oe

**Fig. 4** The real part of the magnetic susceptibility versus the applied field for samples with $x = 0.01$, 0.04, 0.06, and 0.1 wt% at $T = 42$ K

transport properties of ceramic superconductors are strongly related to the microstructure of these granular materials, where the intrinsic superconducting properties of the grains are strongly modified by the grain coupling effects. The observed peculiar broadness in the $\chi'(T)$ curves could be explained due to changes in the grain orientations, grain size, and grain boundaries of Gd-123 during the process of preparation [34]. As shown from SEM micrographs, some grains are unfavorably oriented which may be the reason for broadness in the $\chi'(T)$ curves. The results are consistent with the results shown in SEM micrographs in previous studies [28]. Through the variation of $\chi'$ versus temperature, it is possible to obtain $T_c$ as the temperature at which $\chi'$ changes from a positive to a negative value [35]. The values of $T_c$ for superconducting samples $(CoFe_2O_4)_x GdBa_2Cu_3O_{7-\delta}$, for $0 \leq x \leq 0.1$ wt%, at $H = 9$ Oe are listed in Table 1. It was observed that the value of $T_c$ decreases as $x$ increases. The decrease in $T_c$ is probably due to the trapping of mobile free carriers and non-uniform distribution of nanoparticles [36] at grain boundaries of the host Gd-123 phase and the copper pair breaking mechanism supported by the high concentration of nanoparticles [37]. It is clear the diamagnetism factor increases up to $x = 0.01$ wt% and then it decreases for $x = 0.01$ wt%. As the concentration of the nanosized $CoFe_2O_4$, $x > 0.01$ wt%, gets higher, the composition at the termination ends of the crystal may be altered. Subsequently, this will increase the

normal-state resistivity of the material and the inadvertent phase formation at the termination ends of the crystal. Thus, the formation of this phase would suppress the magnitude of the diamagnetism of the final compound [38].

The temperature variation of $\chi'(T)$ at different applied dc magnetic fields, for $(CoFe_2O_4)_{0.06}GdBa_2Cu_3O_{7-\delta}$, is shown in Fig. 2. The superconducting transition temperature shifts to lower values with increase of the applied dc magnetic field. The Meissner fraction is found to decrease with increase of the applied fields. Figure 3 shows the variation of $\chi'$ versus temperature $(d\chi'/dT)$ at selected dc magnetic fields ($H = 0$, 100, 1000, and 3000 Oe). The figure clearly shows that there is a knee at low applied fields at $T$ from 70 to 80 K. This knee disappears at high applied magnetic fields. It is well known that magnetization in a superconductor arises from diamagnetic shielding, trapped flux, and paramagnetic contribution from Cu in the matrix. The appearance of the knee at lower fields is probably due to the relative increase of magnetic contribution from the Cu in the matrix comparing to the effects of diamagnetic shielding and trapped flux.

Figure 4 shows the magnetic field dependence of $\chi'$ for $(CoFe_2O_4)_x GdBa_2Cu_3O_{7-\delta}$ ($x = 0$, 0.01, 0.04, 0.06, and 0.08 wt%) at $T = 42$ K. The magnetic field dependence of $\chi'$ is almost linear, where the slopes $(d\chi'/dH)$ are considered as the rate of the shift in the magnitude of the Meissner fraction with the applied field. The equations of linear fit of the $\chi'-H$ graphs are reported in Table 2. The lowest value of slopes is found at $x = 0.01$ wt%, indicating that this sample strongly resists the field and it has more flux pinning ability [32]. These results are consistent with the increase of the critical magnetic fields ($B_C$, $B_{C1}$, and $B_{C2}$) and the critical current density $J_c$ with $x = 0.01$ wt% nanosized $CoFe_2O_4$ [28].

The temperature dependence of $\chi''(T)$ at different applied dc magnetic fields for $(CoFe_2O_4)_{0.06}GdBa_2Cu_3 O_{7-\delta}$ is shown in Fig. 5. The curves $\chi''$ show only the intergrain peak and the disappearance of the intragranular peak. The missing of the intragrain peak is due to overlapping with the much broader intergrain peak. This observation indicates that the loss within the Gd-123 samples occurs at fields greater than that of Y-123 samples. This also shows that the applied dc magnetic field is not sufficient to penetrate the intragrain superconductors, signifying good electrical contacts between the superconducting grains. These results are consistent with those obtained by

| **Table 2** Fitting relations of $\chi'$ as a function of $H_{dc}$ for $(CoFe_2O_4)_x GdBa_2Cu_3O_{7-\delta}$, $x = 0.001$, 0.04, 0.06, and 0.1 wt% | | | |
|---|---|---|---|
| | $x = 0.01$ | $\chi' = 1.89 \times 10^{-6}H - 0.01212$ | $R^2 = 0.9795$ |
| | $x = 0.04$ | $\chi = 2.721 \times 10^{-6}H - 0.01565$ | $R^2 = 0.9111$ |
| | $x = 0.06$ | $\chi = 2.78 \times 10^{-6}H - 0.01565$ | $R^2 = 0.9175$ |
| | $x = 0.1$ | $\chi = 2.22 \times 10^{-6}H - 0.0081$ | $R^2 = 0.9872$ |

**Fig. 5** The imaginary part of the magnetic susceptibility of samples with $x = 0.06$ wt% for applied dc field values 0 Oe $\leq H_{dc} \leq 3000$ Oe
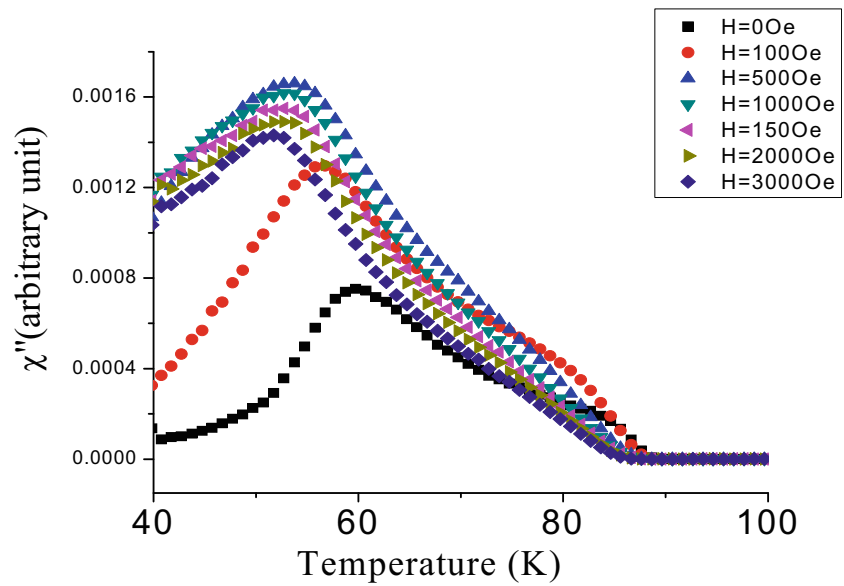


Namuco et al. [33] and Rojas et al. [39] for the Gd-123 phase. The intergranular loss peak at $T_P$ shifts to a lower temperature with the increase of the applied dc magnetic field. This is probably due to the losses associated to the motion of an intergranular Josephson junction [40]. It is clear that the height of intergranular peaks increases as the applied dc magnetic field increases up to 1000 Oe and then it decreases with further increase of the applied dc magnetic field. The shift of $T_P$ as a function of the applied dc field $\left(\frac{\Delta T_P}{\Delta H}\right)$ decreases from 0.2 to 0.13 % as $x$ increases from 0 to 0.01 wt%, and then it increases to 0.33 % for $x = 0.1$ wt%. This means that the larger shift corresponds to the weaker pinning [41] in agreement with our previous results that showed that $B_{C1}$, $B_{C2}$, and $J_c$ have the highest value at $x = 0.01$ wt% [28].

In order to analyze the temperature dependence of the irreversibility line, we plot the logarithmic plot between the applied dc field with $[1 - T_{irr}/T_0]$, where $T_{irr}$ is the temperature at which $\chi''$ is maximum in the presence of a certain applied magnetic field and $T$ is that temperature without an applied field, for $(CoFe_2O_4)_x GdBa_2Cu_3O_{7-\delta}$ compounds with $x = 0.04$, $x = 0.06$, and $x = 0.08$ wt%. These results are shown in Fig. 6. The results are well fitted according to the following relation:

$$H_{irr} = [1 - T_{irr}/T_0]^n \qquad (1)$$

The values of $n$ vary from one HTSC family to another and are usually between 1.5 and 5.5. This is related to the degree of anisotropy of the system [42]. The fitting shows a power law dependence over all ranges of data but with different exponents, indicating the difference between the behavior at low and high field regions. The values of $n_1$ (for $H < 1000$ Oe) and $n_2$ (for $H \geq 1000$ Oe), obtained from fitting of the

experimental data according to (1), are listed in Table 1. The values of $n_1$ are larger than the values obtained for Y-123 [43] and for Gd-123 added with $ZnFe_2O_4$ [30]. The values of $n_2$ are closer to those obtained for the Hg-1234 system [44] and for Gd-123 added with $ZnFe_2O_4$ [30].

The proposed theoretical interpretation for the nature of $H_{irr}$ includes thermal depinning [45] and vortex glass transition [46]. The exponential dependence of $T_{irr}$ at low fields is interpreted in terms of thermal depinning [45]. At higher fields, $H_{irr}$ is explained in terms of a thermally activated 3D–2D crossover [47] and glass transition [48]. The logarithmic plot of $H_{irr}$ versus $(1 - T_{irr}/T_0)$ showed a crossover at a field of 1000 Oe which is larger than the crossover field of 500 Oe for Gd-123 added with $ZnFe_2O_4$ [30]. Matsushita [49, 50] introduced a model based on a depinning mech-
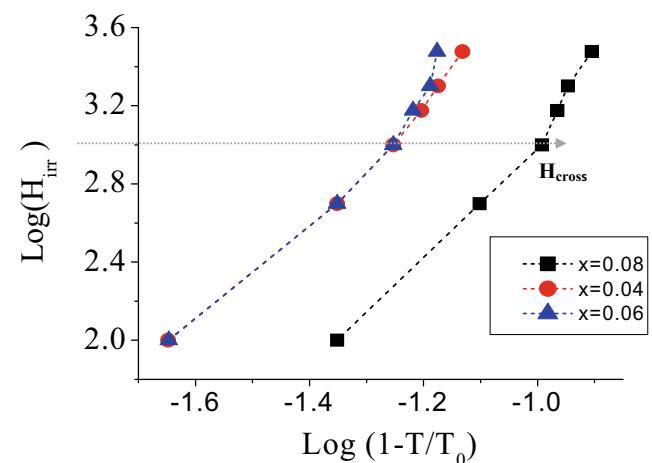


**Fig. 6** Log ($H_{irr}$) versus log $(1 - T_{irr}/T_c)$ for $(CoFe_2O_4)_x GdBa_2Cu_3O_{7-\delta}$ with $x = 0.04$, 0.06, and 0.08 wt%
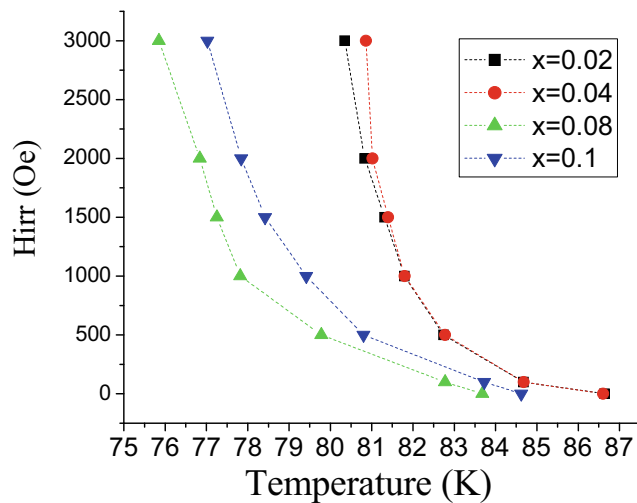
**Fig. 7** Fitting of $H_{\text{irr}}$ versus $T$ by Matsushita's formula for $(ZnFe_2O_4)_x GdBa_2Cu_3O_{7-\delta}$ with $x = 0.02$, 0.04, 0.08, and 0.1 wt%

anism caused by thermally activated flux creep which is expressed by the following equation:

$$H_{\text{irr}} = \left(\frac{K}{T}\right)^{\frac{4}{3-2\gamma}} \left[1 - \left(\frac{T}{T_c}\right)^2\right]^{\frac{2m}{3-2\gamma}}, \qquad (2)$$

where $K$, $m$, and $\gamma$ are numerical parameters of the theory dependent on the creep-free pinning force and current density. The experimental result with the fitting according to (2) for $(CoFe_2O_4)_x GdBa_2Cu_3O_{7-\delta}$ compounds with $x = 0$, 0.02, 0.04, 0.08, and 0.1 wt% and the fitted data are shown in Fig. 7. It is clear that the experimental results are well fitted to (2) with the best parameters $K$, $m$, and $\gamma$ which are listed in Table 1. The values of $K$, $m$, and $\gamma$ are consistent with the results obtained for Gd-123 added with $ZnFe_2O_4$ nanoferrite [30].

## 4 Conclusions

The effect of dc magnetic fields up to 3000 Oe on $(CoFe_2O_4)_x GdBa_2Cu_3O_{7-\delta}$ has been studied. It was found that the addition of the nanosized $(CoFe_2O_4)_x$ increased the superconducting transition temperature up to $x = 0.01$ wt%, and then, it decreased with further increase of $x$. The logarithmic plots of $H_{\text{irr}}$ versus $(1 - T_{\text{irr}}/T_c)$ showed a crossover at a field $H_{\text{dc}} = 1000$ Oe, reflecting a transition from 2D to 3D vortex fluctuations. Moreover, the $H_{\text{irr}}-T$ curves were well fitted with Matsushita's formula, indicating a thermally activated flux creep behavior.

## References

1. Reddy, P., Shekar, S., Somaiah, K.: J. Mater. Lett. **21**, 21–29 (1994)
2. Zhang, Y.F., Izumi, M., Li, Y.J., Murakami, M., Gao, T., Liu, Y.S., Li, P.L.: Phys. C **471**, 840 (2011)
3. Sakai, N., Lee, S., Chikumoto, N., Izumi, T., Tanabe, K.: J. Phys. C **471**, 1075 (2011)
4. Nariki, S., Sakai, N., Murakami, M.: Phys. C **341–348**, 2409 (2000)
5. Harada, T., Yoshida, K.: Phys. C **383**, 48 (2002)
6. Wahl, A., Hervieu, M., Vantendeloo, G., Hardy, V., Provost, J., Groult, D., Simon, C., Raveau, B.: Radiat. Eff. Defects Solids **133**, 293 (1995)
7. Weber, H.W., Wiesinger, H.P., Kritscha, W., Sauerzopf, F.M., Crabtree, G.W., Liu, J.Z., Chang, Y.C., Jiang, P.Z. Adam. Hilger Ltd, Bristol (1991)
8. Safar, H., Cho, J.H., Fleshler, S., Maley, M.P., Willis, J.O., Coulter, J.Y., Ullmann, J.L., Lisowski, P.W., Riley, G.N., Rupich, M.W., Thompson, J.R., Krusinelbaum, L.: J. Appl. Phys. Lett. **67**, 130 (1995)
9. Giapintzakis, J., Lee, W.C., Rice, J.P., Ginsberg, D.M., Robertson, I.M., Wheeler, R., Kirk, M.A., Ruault, M.O.: J. Phys. Rev. B. **45**, 10677 (1992)
10. Hart, H.R., Luborsky, F.E., Arendt, R.H., Fleischer, R.L., Tkaczyk, J.E., Orsini, D.A.: IEEE Trans. Magn. **27**, 1375 (1991)
11. Weinstein, R., Sawh, R.-P.: Phys. C: Supercond. **383**, 438 (2003)
12. Dou, S.X., Wang, X.L., Guo, Y.C., Hu, Q.Y., Mikheenko, P., Horvat, J., Ionescu, M., Liu, H.K.: J. Supercond. Sci. Technol. **10**, A52 (1997)
13. Bardeen, J., Stephen, M.J.: Phys. Rev. **140**, 1197 (1965)
14. Dou, S.X., Wang, X.L., Guo, Y.C., Hu, Q.Y., Mikheenko, P., Horvat, J., Ionescu, M., Liu, H.K.: J. Supercond. Sci. Technol. **10**, A52 (1997)
15. Abdeen, W., Mohammed, N.H., Awad, R., Mahmoud, S.A., Hasebbo, M.: J. Supercond. Nov. Magn. **26**, 623 (2013)
16. Kong, W., Abd-Shukor, R.: J. Supercond. Nov. Magn. **23**, 257 (2010)
17. Mawassi, R., Marhaba, S., Roumié, M., Awad, R., Korek, M., Hassan, I.: J. Supercond. Nov. Magn. (2013). doi:10.1007/s10948-013-2408-9
18. Lei, L., Zhao, G., Xu, H., Wu, N., Chen, Y.: Mater. Chem. Phys. **127**, 91 (2011)
19. Elokr, M.M., Awad, R., Abd El-Ghany, A., Abou Shama, A., Abd El-wanis, A.: J. Supercond. Nov. Magn. **24**, 1345 (2011)
20. Abou-Aly, A.I., Abdel Gawad, M.M.H., Awad, R., G-Eldeen, I.: J. Supercond. Nov. Magn. **24**, 2077 (2011)
21. Abou-Aly, A.I., Mohammed, N.H., Awad, R., Motaweh, H.A., El-Said Bakeer, D.: J. Supercond. Nov. Magn. **25**, 2281 (2012)
22. Moutalbi, N., Ouerghi, A., Djurado, E., Noudem, J.G., M'chirgui, A.: Phys. C **471**, 97 (2011)
23. Yildirim, G.: J. Alloys Compd. **578**, 526 (2013)
24. Khan, N.A., Aziz, S.: J. Alloys Compd. **538**, 183 (2012)
25. Xu, C., Hu, A., Ichihara, M., Sakai, N., Hirabayashi, I., Izumi, M.J.: Phys. C **460–462**, 1341 (2007)
26. Xu, C., Hu, A., Sakai, N., Izumi, M., Hirabayashi, I.J.: Phys. C **445–448**, 357 (2006)
27. Terai, T., Masegi, T., Kusagaya, K., Takahashi, Y., Kishio, K., Motohira, N., Nakatani, K.: Phys. C **185**, 2383 (1991)
28. Abou Aly, A.I., Awad, R., Mohammed, N.H., Motaweh, H.A., El-Said Bakeer, D.: J. Supercond. Nov. Magn. **25**, 2281–2290 (2012)
29. Roa-Rojas, J., Menegotto Costa, R., Pureur, P., Prieto, P.: Phys. Rev. B **61**, 12457 (2000)
30. Abou Aly, A.I., Awad, R., Rouie, M., Esper, S., Basma, H.: J. Supercond. Nov. Magn. **28**, 535–539 (2015)

31. Abou Aly, A.I., Awad, R., Mohammed, N.H., Motaweh, H.A., El-Said Bakeer, D.: J. Alloys Compd. **27**, 1757–1767 (2014)
32. Bahgat, A.A., Shaisha, E.E., Saber, M.M.: Phys. B **399**, 70 (2007)
33. Namuco, S.B., Lao, M.L., Sarmago, R.V.: J. Phys. Procedia **45**, 169–172 (2013)
34. Veneva, A., Iordanov, I., Toshev, L., Stoyanova-Ivanova, A., Gogova, D.: Phys. C **308**, 175 (1998)
35. Lombardo, L.W., Mitzi, D.B., Kapitulnik, A., Leone: Phys. Rev. B **46**, 5615 (1992)
36. Khan, N.A., Mumtaz, M., Ullah, A., Hassan, N., Khurram, A.A.: J. Alloys Compd. **507**, 142 (2010)
37. Barik, H.K., Ghorai, S.K., Bhattacharya, S., Kilian, D., Chaudhuri, B.K.: J. Mater. Res. **15**, 1076 (2000)
38. Khan, N.A., Saleem, A., Hussain, S.T.: J. Supercond. Nov. Magn. **25**, 1725 (2012)
39. Roa-Rojas, J., Menegotto Costa, R., Pureur, P.: J. Phys. Rev. B **61**, 457–462 (2000)
40. Ramachandran, J.S., Huang, M.X., Bhagat, M.S., Kish, K., Tyagi, S.: Phys. C **202**, 151 (1992)
41. Celebi, S., Kolemen, U., Malik, A.I., Ozturk, A.: Phys. Stat. Sol. A **194**, 260 (2002)
42. Chank, Liou, S.H.: J. Phys. Rev. B **45**, 5547 (1992)
43. Xu, W., Suenaga: J. Phys. Rev. B **43**, 5516 (1991)
44. Kim, D.H., Gray, K.E., Kampwirth, R.T., Smith, J.C., Richardson, T.J., Kang, J.H., Talvacchio, J., Eddy, M.J.: Phys. C **177**, 431 (1991)
45. Yeshurn, Y., Malozemoff, A.: J. Phys. Rev. Lett. **60**, 2202 (1987)
46. Fisher, M.P.A.: J. Phys. Rev. Lett. **62**, 1415 (1989)
47. Miu, L.: J. Phys. Rev. B **46**, 1172 (1992)
48. Safar, H., Gammel, P.L., Bishop, D.: J. Phys. Rev. Lett. **68**, 2672 (1992)
49. Matsushita, T.J.: Phys. C **205**, 289 (1993)
50. Matsushita, T.J.: Phys. C **164**, 150 (1990)